Perturbations in Factor XIII Resulting from Activation and Inhibition Examined by Solution Based Methods and Detected by MALDI-TOF MS†

T. Michael Sabo, P. Bradley Brasher, and Muriel C. Maurer*

Department of Chemistry, University of Louisville, Louisville, Kentucky 40292

Received March 26, 2007; Revised Manuscript Received May 29, 2007

ABSTRACT: Factor XIII can be activated proteolytically by thrombin cleavage of the activation peptide or non-proteolytically by exposure to 50 mM Ca^{2+}. The resultant transglutaminase cross-links Q and K residues within the noncovalently associated fibrin clot. Hydrogen deuterium exchange coupled with MALDI-TOF MS demonstrated that FXIII activation protects regions within the β sandwich (98−104) and the β barrel 1 (526−546) from deuterium, while exposing the potential Q substrate recognition site (220−230) to deuteration (Turner, B. T., Jr., and Maurer, M. C. (2002) *Biochemistry 41*, 7947−7954). Chemical modification indicated the availability of several residues upon activation including K^{73}, K^{221}, C^{314}, and C^{409} (Turner, B. T., Jr., Sabo, T. M., Wilding, D., and Maurer, M. C. (2004) *Biochemistry 43*, 9755−9765). In the current work, activations of FXIII by IIa and by Ca^{2+} as well as FXIIIa inhibition by the K9 DON peptide (with the Q isostere 6-diazo-5-oxo-norleucine) and iodoacetamide were further examined. New findings unique for $FXIIIa^{IIa}$ included alkylation of C^{238} and C^{327}, acetylation of K^{68}, and increased proteolysis of 207−214. By contrast, $FXIIIa^{Ca}$ led to increased proteolysis of 73−85 and 104−125 and to a loss of K^{129} acetylation. The FXIIIa inhibitors K9 DON and iodoacetamide both promoted even greater protection from deuteration for the β sandwich (98−104) and β barrel 1 (526−546). Interestingly, only K9 DON was able to block modification of catalytic core C^{409} near the dimer interface. The solution based approaches reveal that activation and inhibition lead to local and long range effects to FXIII(a) and that many are influenced by Ca^{2+} binding. Important glimpses are being provided on FXIIIa allostery and the presence of putative FXIIIa exosites.

Blood coagulation culminates with the action of three proteins: thrombin, fibrinogen, and factor XIII (FXIII[1]). Conversion of fibrinogen to fibrin results from thrombin (IIa) cleavage of fibrinopeptides A and B from fibrinogen, leading to noncovalent association and a soft clot (*1*, *2*). IIa also activates FXIII, and the resultant transglutaminase (TGase) covalently cross-links fibrin monomers through the formation of isopeptide bonds between Q and K residues (*3*). These covalent bonds act to stabilize the growing clot. Furthermore, FXIIIa aids in protecting the clot from plasmin degradation through the incorporation of substrates, such as α_2 antiplasmin (*4*), to the fibrin matrix.

FXIII shares the same primarily β sheet architecture of the other known TGases (*5*). The four principal structural elements of the TGase family are depicted in Figure 1A: the β sandwich, the catalytic core, and the β barrel 1 and 2 domains. The active site architecture for both cysteine proteases and TGases are quite similar, consisting of the catalytic triad C^{314}, H^{373}, and D^{396} (FXIII numbering) (Figure 1B); however, the proposed mechanism of TGases is the reverse of cysteine proteases (*5*, *7*). The only TGase to exist as a dimer is FXIII, with key interchain interactions between K^{113}−$D^{367'}$, K^{257}−$E^{401'}$, and R^{260}−$D^{404'}$ (Figure 1B).

Catalytically competent FXIIIa is achieved when IIa cleaves the N-terminal activation peptide, and at least 1 mM Ca^{2+} is present (*8*, *9*). After proteolysis by IIa, the activation peptide remains noncovalently associated with FXIIIa and transverses both monomers (Figure 1A) (*10*). Alternatively, high concentrations of Ca^{2+} (>50 mM) or of monovalent cations (150 mM−1 M) with 1 mM Ca^{2+} can non-proteolytically activate FXIII (*11*, *12*). Only one Ca^{2+} binding site (Figure 1B) has been observed (N^{436}, D^{438}, A^{457}, E^{485}, and E^{490}) (*13*), though the existence of several more low affinity sites has been supported by equilibrium dialysis (*14*) and ^{43}Ca NMR (*15*).

Interestingly, alkylation of C^{314} by a small molecule such as iodoacetamide (IAA) occurs only after activation (*9*, *12*, *16*, *17*). Yet, the X-ray structures of zymogen (*5*), $FXIIIa^{IIa}$ (*10*), and $FXIIIa^{Ca}$ (*13*) are lacking in significant rmsd deviations (*10*). These observations led Yee et al. to hypothesize that the inactive and active conformers exist in equilibrium (*13*). Since the inactive conformer is favored during crystallization, FXIIIa interaction with a substrate or inhibitor may favor crystallization of the active conformer (*13*). Recently, Hausch et al. have reported the inhibition of

† Funding for this project was provided by NIH Grant R01 HL68440.

* To whom correspondence should be addressed. Tel: 502-852-7008. Fax: 502-852-8149. E-mail: muriel.maurer@louisville.edu.

[1] Abbreviations: FXIII, recombinant human cellular Factor XIII; FXIII(a), unactivated or activated Factor XIII; $FXIIIa^{Ca}$, calcium activated Factor XIII; $FXIIIa^{IIa}$, thrombin activated Factor XIII; IIa, thrombin; TGase, transglutaminse; IC_{50}, concentration of inhibitor that causes 50% inhibition; IAA, iodoacetamide; DON, 6-diazo-5-oxo-norleucine; NEM, *N*-ethylmaleimide; MALDI-TOF MS, matrix-assisted laser desorption-ionization time-of-flight mass spectrometry; HDX, hydrogen−deuterium exchange; GDH, glutamate dehydrogenase; GEE, glycine ethyl ester; PPACK, D-Phe-Pro-Arg-chloromethylketone.

10.1021/bi700579z CCC: $37.00
Published on Web 08/11/2007

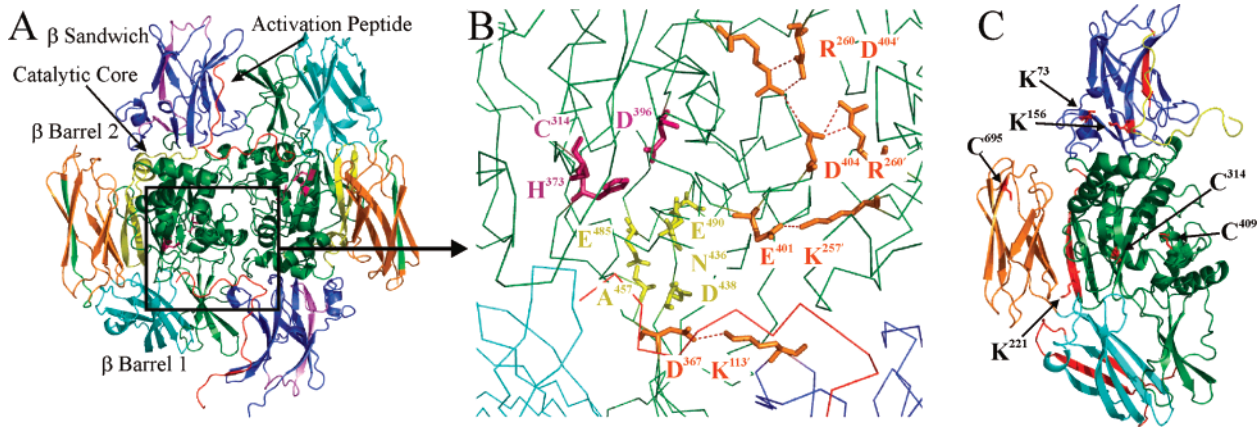

FIGURE 1: (A) TGase Factor XIII depicted as the A_2 dimer from the X-ray crystal structure 1FIE (*10*). Color coded regions include the activation peptide (red), β sandwich (blue), catalytic core (green), β barrel 1 (cyan), and β barrel 2 (orange). The catalytic triad residues (C^{314}, H^{373}, and D^{396}) are highlighted in pink. The two Q substrate recognition sites peptide 4, within the β sandwich, and peptide 7, within the catalytic core, are purple and yellow, respectively. The potential K substrate recognition site in β barrel 2 is light green. (B) Expanded view of the catalytic core and the dimer interface. Depicted in the figure are the active site (violet), the Ca^{2+} binding site (yellow), and key interactions at the dimer interface (orange). (C) Summary of previous results with residues and peptides experiencing conformational changes upon FXIII activation highlighted in red. β sandwich (blue): (1) 98−104 large decrease in % deuteration upon Ca^{2+} activation. (2) K^{73} acetylated within peptide 4 upon Ca^{2+} activation. (3) K^{156} acetylated upon IIa activation. Catalytic core (green): (1) 220−230 increase in % deuteration. (2) K^{221} acetylated within peptide 7. (3) C^{314} is alkylated. (4) C^{409} alkylated at the dimer interface. β barrel 1 (cyan): (1) 513−522 small decrease in % deuteration. (2) 526−546 large decrease in % deuteration upon Ca^{2+} activation. β barrel 2 (orange): (1) C^{695} is alkylated. These figures were created using PyMol (*6*).

tissue TGase 2 with gluten peptide analogues that replace glutamine with the Q isostere 6-diazo-5-oxo-norleucine (DON) (*18*) (Figure 2A). The DON moiety has now been incorporated into the FXIIIa substrate K9, which is a peptide derived from β casein (*19*). By inhibiting FXIIIa with a peptide, solution based studies could potentially yield clues on how FXIIIa interacts with proteins containing a reactive Q and how this TGase prepares for K substrate incorporation. Currently, a crystal structure of an inhibited TGase or a TGase interacting with a ligand has not been solved.

Several prospective FXIII(a) exosites have been proposed. An exosite is a ligand−protein interface that is distinct from the residues involved in catalysis. Exosite functions include guiding substrate orientation for more efficient catalysis and/or providing a separate cofactor interaction site that either enhances or dampens enzyme reactivity. Two potential Q substrate exosites, peptides 4 (72−97) and 7 (190−230), are located within the β sandwich and the catalytic core, respectively (Figure 1A) (*20*). Peptides derived from these sequences competitively inhibit Q substrate catalysis. Within β barrel 2, the antibody 5A2 targets residues 646−658 and acts as a competitive inhibitor of K substrate incorporation. Such β barrel 2 residues may thus be part of a K substrate exosite (*21*). The different studies mentioned above support the use of peptides and antibodies in elucidating how substrates are recognized by FXIIIa.

Previous work in this lab has focused on implementing solution based methods to probe the conformational dynamics of FXIII activation that may be undetected in static X-ray crystal structures (*22*, *23*). Two useful techniques for observing protein dynamics are hydrogen−deuterium exchange (HDX) of backbone amide protons analyzed by MALDI-TOF MS and differential chemical modification of C and K residues. Figure 1C summarizes previous results using these techniques. HDX studies have revealed potential allostery associated with Ca^{2+} binding for both the β sandwich and β barrel 1 domains. Furthermore, activating FXIII was determined to expose regions within the proposed exosite peptides 4 and 7 (*20*) to modify C^{409} at the A_2 dimer interface and to affect the conformation of β barrel 2. These studies highlight the subtle conformational changes that are associated with the activation of FXIII.

The focus of the present work is two-fold. First, further studies were performed examining the conformational perturbations that result from proteolytic activation by IIa ($FXIIIa^{IIa}$) versus nonproteolytic activation with 50 mM Ca^{2+} ($FXIIIa^{Ca}$). K^{68} acetylation and increased proteolysis of 207−214 by chymotrypsin imply additional peptide 7 exposure associated with IIa activation. Regarding $FXIIIa^{Ca}$, unique changes in the dynamics of the β sandwich and the β barrel 2 may suggest the presence of additional Ca^{2+} binding sites. The second facet of these studies concerned FXIIIa inhibition. For the first time, the FXIIIa inhibitors IAA and K9 DON were investigated using the described techniques. A TGase activity assay demonstrated that K9 DON inhibits FXIIIa with an IC_{50} in the high nanomolar range. HDX then revealed that a β sandwich fragment and several regions within β barrel 1 were further stabilized by inhibition of FXIIIa. NEM studies showed that only inhibition with K9 DON abrogates C^{409} alkylation near the catalytic triad. Acetic anhydride studies indicated that in $FXIIIa^{Ca}$ K9 DON inhibition blocked modification of K^{482}. These investigations have demonstrated the efficacy of the DON moiety as an inhibitor specific for FXIIIa. More importantly, potential regions of plasticity resulting from activation and inhibition of FXIIIa have been observed that appear static in the currently available crystal structures.

MATERIALS AND METHODS

Factor XIII Preparation and Synthetic Peptides. Recombinant human cellular factor XIII (FXIII) was a generous gift from Dr. Paul Bishop (ZymoGenetics, Inc., Seattle, WA) (*24*). Lyophilized FXIII was reconstituted in 18 MΩ deionized water. The concentration of FXIII was determined with a Cary 100 UV/vis spectrophotometer monitoring absorbance

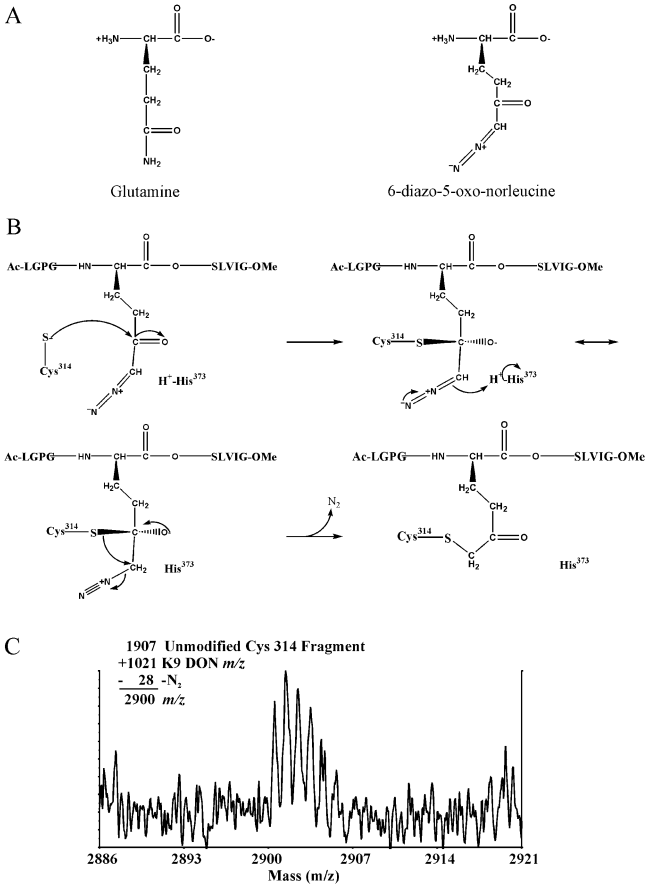

FIGURE 2: K9 DON Inhibition of FXIIIa. (A) Isosteres glutamine and 6-diazo-5-oxo-norleucine. (B) Proposed mechanism of inhibition (*27*) proceeds through tetrahedral intermediate formation resulting from cysteine attack at the carbonyl group. The methylene carbon then abstracts a proton from the active site H^{373}. Finally, a thioether is formed resulting in the release of N_2 and irreversible inhibition of FXIIIa. (C) Representative mass spectra of the K9 DON modified C^{314} fragment from a tryptic digest.

at 280 nm and using the FXIII extinction coefficient of 1.49 mL/mg cm. Aliquots of 40 μM FXIII were stored at -70 °C.

K9 is a peptide substrate for FXIIIa that is derived from β casein (*19*). The sequence of K9 is Ac-LGPGQSKVIG-OMe and was synthesized by Peptides International (Louisville, KY). The active site inhibitor Ac-LGPG-(DON)-SLVIG-OMe (K9 DON) was custom synthesized by N-Zyme BioTec GmbH (Figure 2A). The K9 DON inhibitor is most soluble at high concentrations in DMSO; therefore, this solvent was used to prepare stock solutions. Experiments where K9 DON is absent contain an equivalent amount of DMSO. Peptide concentrations were determined by quantitative amino acid analysis (AAA Service Laboratory, Inc., Boring, OR).

TGase Assay. The Dade−Behring Berichrom Assay (*19*) utilizes coupled reactions involving FXIIIa and glutamate dehydrogenase (GDH). As FXIIIa reacts with Q from the peptide K9, NH_3 is released. Next, the primary amine glycine ethyl ester (GEE) concludes the TGase reaction through formation of an isopeptide bond with the K9 peptide. GDH converts α-ketoglutarate and NH_3 into glutamate with the aid of reducing equivalents from NADH. Thus, FXIIIa activity is directly related to NADH oxidation, which results in decreasing absorbance at 340 nm.

The FXIII activation mix consisted of 6.9 μM FXIII, 30 nM bovine IIa (purified as described in (*25*)), and 1 mM $CaCl_2$ in 20 mM borate at pH 8.3. After 12 min at 37 °C, IIa activity was inhibited by 376 nM PPACK to prevent further proteolysis of FXIIIa. An additional 12 min at 37 °C elapsed after which 19 μL aliquots of $FXIIIa^{IIa}$ were made and stored at -70 °C.

Inhibition of $FXIIIa^{IIa}$ with either K9 DON or iodoacetamide (IAA) was monitored with a modified version of the Berichrom assay (*26*). Figure 2B illustrates the proposed mechanism for inhibition of FXIIIa by K9 DON, and Figure 2C displays the mass spectrum indicating K9 DON modification of C^{314} (*27*). Irreversible inhibition is a time and concentration dependent phenomena. Throughout each trial, the volumes of the detector reagent (250 μL) and the activator reagent (163 μL) as well as $FXIIIa^{IIa}$ (218 nM) and K9 peptide (313 μM), in 100 mM bicine at pH 8.3, were held constant. The amount of the inhibitor K9 DON or IAA ranged from 0 to 5000 nM, resulting in inhibitor to FXIIIa active site molar ratios of 1:1 to 23:1. The assay contents were incubated in a Cary 100 UV/vis spectrophotometer for 5 min at 37 °C, then the substrate K9 was added. NADH oxidation was monitored for 10 min at 340 nm. Since 4% DMSO is present in the assay mix, a series of control experiments were performed, demonstrating that $FXIIIa^{IIa}$ in 4% DMSO possesses identical activity to $FXIIIa^{IIa}$ with an equal amount of dI water (data not shown).

$FXIIIa^{IIa}$ activity was measured by determining the slope for the steepest part of the curve. The slope represents the velocity of the reaction (Δabs/min). The resultant slope of $FXIIIa^{IIa}$ activity in the absence of the inhibitor was assigned as 0% inhibition or 100% activity. All reaction velocities calculated in the presence of K9 DON or IAA were normalized with respect to the slope observed with 0% inhibition. As described in Rajagopal et al. (*28*), IC_{50} values for inhibition of $FXIIIa^{IIa}$ were determined by plotting the % inhibition versus the log of the inhibitor concentration, which produced an apparent sigmoidal curve. The following equation was used to fit the sigmoidal with SigmaPlot:

$$\%\ \text{inhibition} = a + \frac{(b + a)}{1 + \left(\frac{\log([\text{inhibitor}])}{\text{IC}_{50}}\right)^{c}} \qquad (1)$$

where *a* represents the minimal curve asymptote, *b* equals the maximal curve asymptote, and *c* is the Hill slope, which is an indicator of the steepness of the inhibitor−response curve.

Activation and Inhibition of FXIII for HDX and NEM Experiments. IIa activation of FXIII proceeded as described for the TGase assay. Ca^{2+} activation of FXIII was carried out in 50 mM $CaCl_2$, 20 mM borate at pH 8.3. The activation mix incubated for 2 h at 37 °C. The inhibitors K9 DON or IAA were added at a 10-fold molar excess to FXIIIa and incubated at 37 °C for 30 min. The Berichrom assay verified FXIIIa activation and inhibition. As seen with uninhibited FXIIIa, K9 DON and IAA inhibited FXIIIa exhibited limited solubility. For the described experiments, enough FXIIIa is present in solution to gather reliable and reproducible results. The design of this mass spectrometry based project hinders our ability to assess whether the inhibitors are binding to

both active sites of the FXIIIa A_2 domain or whether only half-site reactivity is being observed (*16*, *29*). Regardless, we were able to monitor changes in FXIIIa when at least one active site becomes exposed and/or inhibited.

HDX Sample Preparation. FXIIIa was exchanged into 6.67 mM borate and 0.33 mM $CaCl_2$ at pH 8.3, removing excess inhibitor and/or Ca^{2+}. The exception was the standard for comparison, zymogenic FXIII without Ca^{2+}, which was buffer exchanged into 6.67 mM borate at pH 8.3. The concentration of FXIII(a) for all HDX preparations varied from 10 to 13 μM. Aliquots (36 μL) of the buffer exchanged FXIII(a) were evaporated to dryness using a SpeedVac (Savant) and stored at −70 °C.

HDX Experiments. The HDX protocol and analysis have been adapted from methodology developed by the Komives laboratory (*30*−*36*). Dry aliquots of FXIII(a) were allowed to come to room temperature before beginning the experiment. Twelve microliters of 99.996% D_2O (Cambridge Isotope Laboratories) was added to the aliquot yielding 30−36 μM FXIII(a) and 1 mM $CaCl_2$ in 20 mM borate at pH 8.3. The samples were incubated in a desiccator at room temperature for 1 or 10 min. HDX was quenched by adding 120 μL of chilled 0.1% TFA at pH 2.5. Immediately, the entire quenched solution was transferred to a tube of activated pepsin bound to 6% agarose (Pierce Chemical). Digestion occurred on ice for 10 min. Centrifugation at 4 °C separated the digest from the pepsin, and 10 μL aliquots were immediately frozen in liquid N_2 and stored at −70 °C. Each time point was performed three times.

HDX Analysis. A HDX aliquot of FXIII(a) was thawed, immediately mixed with an equal volume of 10 mg/mL α-cyano-hydroxycinnamic acid matrix α(-CHCA) (Aldrich) in 1:1:1 ethanol/CH_3CN/0.1% TFA at pH 2.2, and 0.5 μL was spotted onto a chilled stainless steel MALDI plate. The spotted MALDI plate was dried within a SpeedVac unit and then inserted into the MALDI-TOF MS (Voyager DE-Pro, Applied Biosystems). The entire procedure took about 5 min, limiting the amount of back exchange. Spectra were collected in the reflector mode over a mass range of 800−3500 *m*/*z* with 256 laser shots per spectrum. All peptides in the peptic digest were previously identified by Brian T. Turner, Jr. (*22*) (Supporting Information, Figure S1). Data Explorer (Applied Biosystems) was used to analyze the spectra. Calibration of the spectra involved two singly protonated reference peptides, the monoisotopic mass of 850.4787 Da (residues 535−541), and the quadraisotopic mass of 1375.7097 Da (residues 220−230).

The amount of deuterium uptake by each peptide was quantified as described by Sabo et al. (*37*). Differences in deuteration between the various states of FXIII(a) were calculated utilizing eq 2:

$$\%\ \text{difference} = \left(\frac{D - D_{\text{FXIII}}}{D_{\text{max}}}\right) \times 100\% \qquad (2)$$

where D is the amount of deuterium incorporated in activated or inhibited FXIIIa, D_{FXIII} is the amount of deuterium uptake for zymogen, and D_{max} is the theoretical maximum amount of deuterium incorporation within the indicated peptide. On the basis of previous HDX data analysis, only percent differences larger than 4.5% are considered to be of great significance (*22*, *37*−*39*). The theoretical maximum number of exchangeable protons accounts for all exchangeable backbone amide protons and a slight fraction of N-terminal, C-terminal, and side chain exchangeable protons, which are dependent on the final percentage of D_2O in solution under quench conditions (∼4.5%).

HDX results obtained with the zymogen, $FXIIIa^{Ca}$, and $FXIIIa^{IIa}$ were similar to the work carried out previously (*22*); however, in the past study, portions of the spectrum not related to the actual isotopic cluster were included in calculating the amount of deuterium incorporation. Specifically, the window used in the CAPP program (*30*) for quantification began where the base of the undeuterated monoisotopic peak would appear and ended after the last peak of the longest time point. In this article and a previous publication (*37*), the deuteration was determined by only considering each peak's intensity within the isotopic cluster.

Cysteine Modification with NEM. FXIII(a) at 10 μM was incubated with 50 μM NEM (stock in 50% CH_3CN) for 60 min at room temperature. The reaction was quenched with the addition of dithiothreitol. In either trypsin buffer (100 mM NH_4HCO_3 at pH 8) or chymotrypsin buffer (100 mM Tris-HCl and 10 mM $CaCl_2$ at pH 7.4), the quenched samples were digested with 2 μL of 1 mg/mL chymotrypsin (25 °C) or 1 mg/mL trypsin (37 °C) for at least 4 h. Proteolysis was quenched by acidification with 5% TFA.

Like the HDX experiments, slight differences exist in the results from those already presented (*23*). In the prior study (*23*), the ratio of NEM to FXIII(a) was 200:1. During the course of this investigation, a 50:1 ratio was determined to provide more differential labeling than was previously observed. The results in this work do coincide with those presented in the earlier publication.

Lysine Acetylation and Limited Proteolysis Experiments. In 10 mM NH_4HCO_3 at pH 7.4, FXIII at 10 μM was activated either with Ca^{2+} or with IIa. Inhibition of FXIIIa occurred concurrently with the activation process in the presence of 20 μM IAA or K9 DON in DMSO. Ca^{2+} activation occurred in 50 mM $CaCl_2$ for 2 h at 37 °C. IIa activation took place with 42 nM IIa and 1 mM $CaCl_2$ for 12 min at 37 °C. PPACK was used to inhibit IIa activity and the FXIIIa mix incubated for an additional 108 min.

After 2 h, 5 μL of 600 mM acetic anhydride (AA) in DMF was added to FXIII(a) and allowed to incubate for 1 h. The acetylation mix was acidified with 1% TFA. Residual AA and the byproduct acetic acid were removed by drying in a Speed-Vac concentrator device. When performing limited proteolysis, AA was not added but FXIII(a) was handled in a similar manner. The dry protein was reconstituted in dI water. The modified protein was then split in half and the addition of buffer yielded 10 μM FXIII(a) in 100 mM NH_4HCO_3 at pH 8.0 (trypsin) or in 100 mM Tris-HCl and 10 mM $CaCl_2$ at pH 7.4 (chymotrypsin). To 25 μL of the modified protein in digestion buffer, 2 μL of 1 mg/mL trypsin (37 °C) or chymotrypsin (25 °C) was added, and proteolysis occurred for 4 h. With limited proteolysis, the digest was quenched after 30 min with 5% TFA.

MALDI-TOF Mass Spectrometry for Chemical Modification and Limited Proteolysis. C18 ZipTips (Microcon) were used to concentrate and clean up the digested FXIII(a) samples with elution into 50% CH_3CN. The eluted peptides were mixed with 5 μL of either α-CHCA or ferulic acid

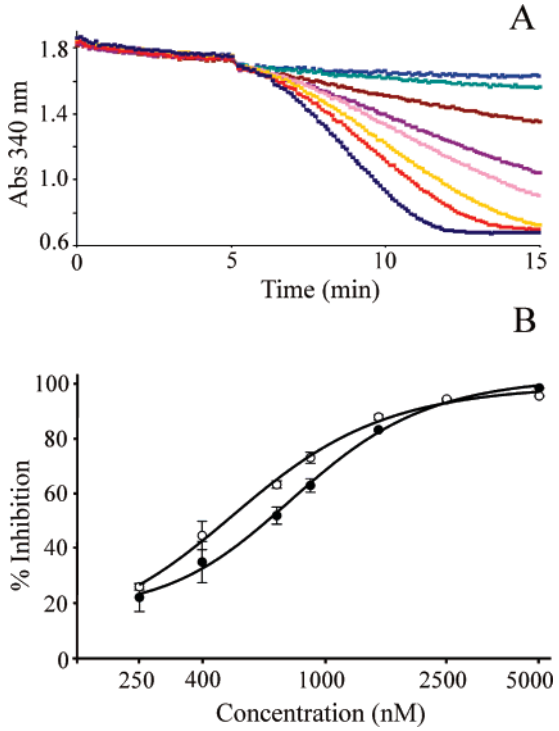

FIGURE 3: TGase assay and FXIIIa inhibition by K9 DON. (A) Eight separate trials were performed at varying inhibitor concentrations: FXIIIa in the absence of K9 DON (navy blue); 250 nM K9 DON (red); 400 nM K9 DON (orange); 700 nM K9 DON (pink); 900 nM K9 DON (purple); 1500 nM K9 DON (brown); 2500 nM K9 DON (cyan); and 5000 nM K9 DON (blue). The assay components, FXIIIa, and the indicated amount of inhibitor were incubated for 5 min at 37 °C, at which point the substrate K9 was introduced to the assay mix. The graph depicts the oxidation of NADH as a function of time. (B) A plot of % inhibition vs the log of inhibitor concentration. Open and filled in circles represent IAA and K9 DON, respectively. Three separate trials were performed, and the plot was fit to eq 1. The IC_{50} was determined as 815.5 ± 31.9 nM for K9 DON and 538.8 ± 74.3 nM for IAA.

MALDI matrix. The samples were spotted on a stainless steel MALDI plate and acquired in reflector mode using MALDI-TOF MS. The mass range was from 550 to 4000 *m/z*, and 256 shots per spectrum were collected. At least three separate trials were performed for each state of FXIII(a) monitored and at least two spectra collected for each trial. All spectra were analyzed as described by Turner et al. (*23*), and the FXIII sequence coverage produced with chymotrypsin and trypsin is presented in Supporting Information, Figure S1. For limited proteolysis, the intensity of a monoisotopic peak representing FXIII(a) digest fragments was normalized with respect to the most intense (abundant) monoisotopic peak. Differences in relative peak intensities greater than 20% were considered significant for the limited proteolysis studies on the basis of a comparative standard employed by Ansong et al. (*40*).

RESULTS

TGase Assay with FXIIIa^{IIa}. A modified version of the Dade−Behring Berichrom assay was performed to determine the potency of the irreversible inhibitor K9 DON for FXIIIa^{IIa} and the results compared to IAA. Figure 3A displays a series of progress curves for inhibition of FXIIIa^{IIa} with increasing concentrations of K9 DON and Figure 3B presents a plot of the data fitted to eq 1. The calculated IC_{50} was 816 ± 32 nM. The small molecular inhibitor IAA was slightly more effective with an IC_{50} of 539 ± 74 nM. The p value comparing the two inhibitors was $p = 0.03$.

Table 1: Changes in Percent Deuteration for Factor XIII−Inhibitor Complexes at 1 and 10 min Relative to Unactivated Factor XIII[a]

	theo	FXIIIa^{Ca}		K9 DON FXIIIa^{Ca}		IAA FXIIIa^{Ca}	
residues	D_{max}[b]	1 m	10 m	1 m	10 m	1 m	10 m
98−104	6.5	**−24.3**[c]	**−15.3**	**−15.5**	**−30.1**	**−31.9**	**−35.0**
220−230	10.8	**5.4**	**9.7**	**7.0**	**7.3**	1.7	**6.2**
240−247	7.5	**6.0**	**7.1**	**7.2**	**5.9**	**6.9**	**8.5**
513−522	9.7	**−11.6**	**−10.6**	**−10.0**	**−11.4**	**−15.6**	**−15.6**
526−546	21.2	**−24.1**	**−25.8**	n/a[d]	**−32.7**	n/a	n/a
535−541	6.5	1.8	2.4	2.6	2.7	1.3	4.2

	theo	FXIIIa^{IIa}		K9 DON FXIIIa^{IIa}		IAA FXIIIa^{IIa}	
residues	D_{max}	1 m	10 m	1 m	10 m	1 m	10 m
220−230	10.8	**4.5**	**7.2**	**5.9**	**6.3**	**6.6**	**7.5**
240−247	7.5	**6.0**	**6.8**	**6.5**	**6.7**	**7.3**	**10.4**
248−264	15.9	**6.0**	3.1	**5.9**	2.2	**6.7**	n/a
513−522	9.7	**−5.4**	**−5.3**	**−7.3**	**−10.3**	**−8.0**	**−9.4**
526−546	21.2	−2.6	−2.4	**−10.0**	**−11.8**	−4.0	**−9.0**
535−541	6.5	1.8	4.2	2.8	**4.9**	2.3	**5.1**

[a] The % change for a particular peptide is calculated by the following equation: % difference = $((D - D_{FXIII})/D_{max}) \times 100\%$, where D is the amount of deuterium incorporated in activated or inhibited FXIII, D_{FXIII} is the amount of deuterium incorporated in the unactivated state, and D_{max} is the theoretical maximum number of exchangeable protons within the indicated peptide. [b] The maximum number of exchangeable protons within the indicated peptide, assuming 100% deuteration. This value accounts for all exchangeable backbone amide protons and a slight fraction of N-terminal, C-terminal, and side chain exchangeable protons, which are dependent on the final percentage of D_2O in solution under quench conditions (~4.5%). A fully deuterated peptide would theoretically have acquired this amount of deuterons. [c] The values in bold represent significant changes in deuteration greater than ±4.5%. [d] n/a refers to a peptide that was either not observed in the peptic digest or was not of sufficient intensity to quantify.

Hydrogen−Deuterium Exchange Coupled with MALDI-TOF Mass Spectrometry. The solvent accessibility of FXIIIa inhibited with IAA or the K9 DON peptide was compared to zymogen, FXIIIa^{Ca}, and FXIIIa^{IIa}. Table 1 contains the differences in deuteration for FXIIIa relative to zymogen, with values greater than ±4.5% in bold text. The table groups the data according to the activation method observed. The amount of deuterium incorporated at each time point is presented in Figure 4 (FXIIIa^{Ca}) and Figure 5 (FXIIIa^{IIa}) as well as in Supporting Information Tables 1 and 2.

The β sandwich residues 98−104 were only present in the FXIIIa^{Ca} spectra, presumably because of pepsin's inability to produce this peptide from FXIIIa^{IIa}. Inhibition of FXIIIa^{Ca} with K9 DON resulted in differences in the deuteration profiles for this peptide at 1 and 10 min. Whereas FXIIIa^{Ca} displayed an increase in solvent accessibility after 10 min (from −24.3% at 1 min to −15.3% after 10 min), K9 DON FXIIIa^{Ca} was observed to acquire less deuterium over a similar time span (from −15.5% at 1 min to −30.1% after 10 min). As for IAA FXIIIa^{Ca}, inhibition with the small molecular inhibitor leads to sustained stabilization over 10 min of deuteration (−31.9% at 1 min to −35.0% after 10 min).

Within the catalytic core, several fragments were observed as displaying similar differences in deuterium exchange,

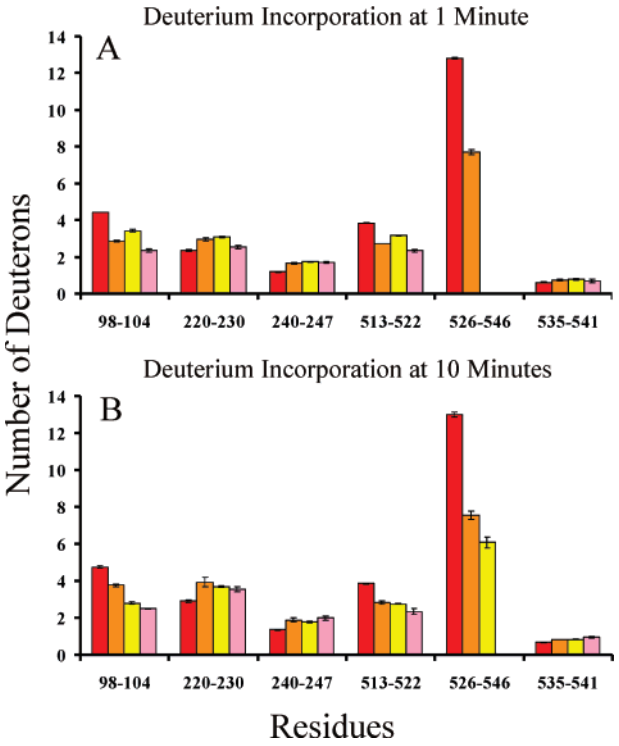

FIGURE 4: Graph of deuterium incorporation at 1 min (A) and 10 min (B) for FXIIIa^{Ca}. The bars in the graph correspond to the following conditions: zymogenic FXIII (red), FXIIIa^{Ca} (orange), K9 DON FXIIIa^{Ca} (yellow), and IAA FXIIIa^{Ca} (pink). Errors correspond to the standard deviation of the mean for three independent trials.

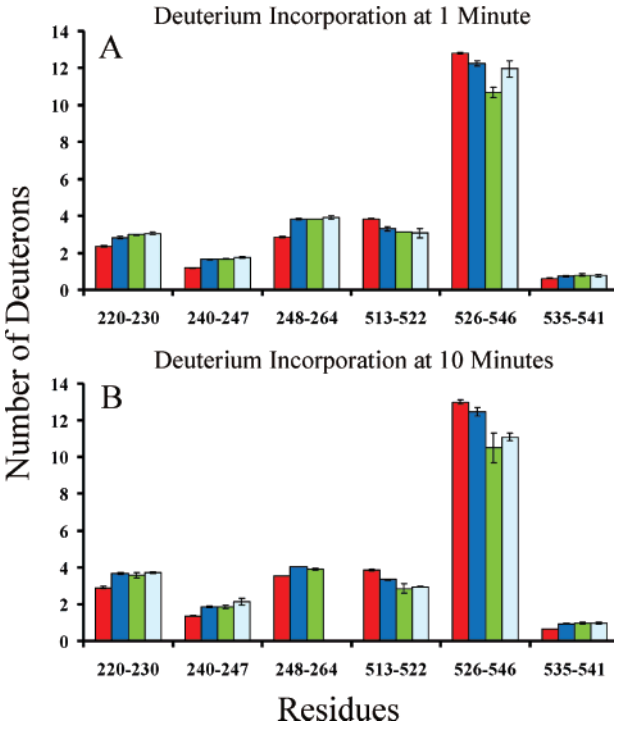

FIGURE 5: Graph of deuterium incorporation at 1 min (A) and 10 min (B) for FXIIIa^{IIa}. The bars in the graph correspond to the following conditions: zymogenic FXIII (red), FXIIIa^{IIa} (blue), K9 DON FXIIIa^{IIa} (green), and IAA FXIIIa^{IIa} (cyan). Errors correspond to the standard deviation of the mean for three independent trials.

regardless of the FXIIIa state monitored. For residues 220−230, deuterium incorporation varied from 4.5 to 7.0% more exposure relative to the zymogen at 1 min, and at 10 min, the range was 6.2−9.7%. The only exception was with IAA FXIIIa^{Ca}, where 1 min of exposure to deuterium did not yield a significant difference in deuteration when compared to that with zymogen (1.7%). Similarly, the results for residues 240−247 were within the standard deviation for all FXIIIa conditions examined: 1 min, 6.0−7.3% and 10 min, 5.9−10.4%. Only FXIIIa^{IIa} presented reliable isotopic clusters for quantification of 248−264. Once again, the type of inhibition when compared to that of FXIIIa^{IIa} had little effect on deuterium exchange. In this case, significant protection was observed initially at 1 min (5.9%−6.7%), and within 10 min, the exchange began to approach zymogenic FXIII (2.2%−3.1%).

The final region of FXIII investigated with HDX was β barrel 1. Considering all FXIIIa^{Ca} states, two of the three regions observed, 513−522 (−10.0% to −15.6%) and 535−541 (1.3% to 4.2%), were similar in regard to the dynamics of deuterium exchange at 1 and 10 min. However, the presence of the K9 DON peptide protects the fragment 526−546 by 6.9% after 10 min of deuteration (−25.8% for FXIIIa^{Ca} and −32.7% for K9 DON FXIIIa^{Ca}). Unfortunately, this region was unable to be observed in the IAA FXIIIa^{Ca} spectra.

When considering the various forms of FXIIIa^{IIa}, residues 513−522 experience slightly more protection from solvent in both inhibited forms of FXIIIa^{IIa}. At 10 min, FXIIIa^{IIa} had incorporated 3.3 deuterons (−5.3%) and both types of inhibited FXIIIa^{IIa} integrated 2.9 deuterons (−9.4% and −10.3%). See Figure 5, Table 1, and Supporting Information, Table 1. The amount of deuterium incorporated in FXIIIa^{IIa} for 526−546 was comparable to that of zymogen (−2.4% to −2.6%). For the same span of residues, K9 DON FXIIIa^{IIa} exhibited an immediate decrease in solvent accessibility after 1 min (−10.0%), and conversely, IAA FXIIIa^{IIa} affected the dynamics of exchange in a gradual manner, reaching a statistically significant difference following 10 min of exchange (−9.0%). Finally, the fragment 535−541 became more exposed to solvent at 10 min in all three forms of FXIIIa^{IIa} (4.2% to 5.1%).

The isotopic clusters representing 526−546 for FXIIIa^{Ca} and K9 DON FXIIIa^{Ca} were of an uneven distribution with a small rise in peak intensity toward higher *m*/*z* (Figure 6). This observation led to a separate series of HDX experiments to be performed on zymogen in the presence of 1 mM Ca^{2+}. The rationale for these HDX trials was to differentiate the effects of Ca^{2+} concentration on deuterium exchange. Figure 6 shows an expanded isotopic cluster for FXIII in 1 mM Ca^{2+}, intermediate between zymogen and FXIIIa^{Ca}, as well as the spectra for the states of FXIIIa^{IIa} in the same region.

N-Ethylmaleimide Modification of FXIII. Digesting FXIII with the proteases trypsin and chymotrypsin provided a total of 81% sequence coverage (Supporting Information, Figure S1). As previously reported (*23*), seven of the nine cysteine residues were able to be observed in the tryptic digests of FXIII: C^{152}, C^{188}, C^{238}, C^{314}, C^{327}, C^{409}, and C^{695}. Unfortunately, chymotrypsin did not produce additional proteolytic peptides containing C^{374} or C^{423}. All NEM modification experiments are summarized in Table 2.

The only consistently unmodified cysteine was C^{152} within the β sandwich. For zymogen, C^{188} was the lone residue to react with NEM. Once FXIII was activated, NEM modified

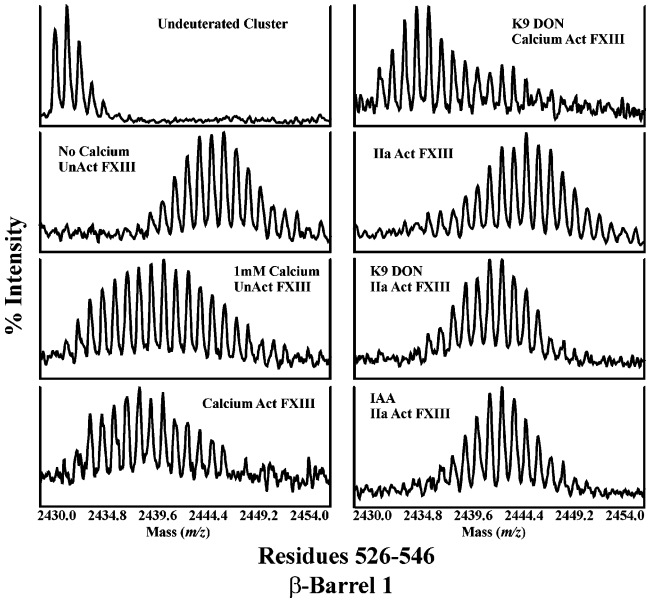

FIGURE 6: Mass spectra representing residues 526−546 (*m*/*z* 2431.534) after 10 min of deuteration. All D-on experiments are in 20 mM borate and 1 mM $CaCl_2$ at pH 8.3, except the zymogen in the absence of Ca^{2+} where the buffer was 20 mM borate at pH 8.3. The FXIII state illustrated in each spectrum is listed in the figure. This peak cluster contains β barrel 1 residues and displays drastically varying degrees of deuteration between $FXIIIa^{Ca}$ and $FXIIIa^{IIa}$. In both types of activation states, inhibition provides protection from solvent amounting to around 1−2 deuterons.

the active site residue C^{314}. Regarding the inhibited forms of FXIIIa, IAA modified C^{314} was observed in the mass spectra (data not shown), and a weak peak for K9 DON covalently linked to C^{314} was infrequently apparent at 2900 *m*/*z* (Figure 2C), probably because of difficulties in ionization.

In the β sandwich, C^{188} was altered by NEM in all three $FXIIIa^{Ca}$ states. Moving to the catalytic core, the residue C^{238} was weakly modified in K9 DON $FXIIIa^{Ca}$, while C^{409} reacted with NEM only when $FXIIIa^{Ca}$ was inhibited by IAA. C^{327} remained unmodified after Ca^{2+} activation. The β barrel 2 residue C^{695} was available to NEM in all three forms of $FXIIIa^{Ca}$. Turning to IIa activation, K9 DON $FXIIIa^{IIa}$ was the only form of $FXIIIa^{IIa}$ to display modification of the β sandwich residue C^{188} and the β barrel 2 residue C^{695}. Two cysteine residues located near the activation peptide, 238 and 327, were consistently labeled in all forms of $FXIIIa^{IIa}$. Finally, the catalytic core C^{409} was modified in $FXIIIa^{IIa}$ and IAA $FXIIIa^{IIa}$; however, K9 DON $FXIIIa^{IIa}$ severely weakened or abrogated chemical modification.

Acetic Anhydride Modification of FXIII. There are 38 lysine residues in FXIII, spanning all four domains. Only 10 of the 38 lysine residues were unable to be observed as acetylated in the mass spectra: K^{61}, K^{269}, K^{363}, K^{366}, K^{418}, K^{445}, K^{446}, K^{462}, K^{467}, and K^{657}. Residues always accessible to acetic anhydride included K^{54}, K^{133}, K^{534}, K^{623}, K^{635}, and K^{704}. Additional labeling of zymogen involved K^{129}, K^{583}, K^{584}, and K^{621}. Lysine residues K^{73}, K^{113}, K^{156}, K^{199}, K^{221}, K^{257}, and K^{531}, were exposed to acetic anhydride only after the activation of FXIII. The modifications recorded from both trypsin and chymotrypsin digests will be combined and the data separated into tables concerning $FXIIIa^{Ca}$ (Table 3) and $FXIIIa^{IIa}$ (Table 4).

In the β sandwich, K^{68} and K^{129} were not accessible to acetic anhydride modification in all forms of $FXIIIa^{Ca}$. Interestingly, the catalytic core K^{482} was labeled in $FXIIIa^{Ca}$ and IAA $FXIIIa^{Ca}$ yet unmodified in K9 DON $FXIIIa^{Ca}$. For all three states of $FXIIIa^{Ca}$, the β barrel 1 residues K^{583}, K^{584}, and K^{621} were modified, while both K^{565} and K^{570} could not be unambiguously assigned as always labeled. Acetylation results revealed that six residues spanning the β sandwich and catalytic core displayed consistent labeling in $FXIIIa^{IIa}$: K^{68}, K^{129}, K^{482}, K^{503}, K^{504}, and K^{513}. Like $FXIIIa^{Ca}$, K^{565}, could not be unambiguously assigned. K^{583} and K^{584} did not react with acetic anhydride when FXIII was activated by IIa; however, general inhibition of $FXIIIa^{IIa}$ resulted in protection from acetic anhydride for the β barrel 1 residue K^{621}.

Limited Proteolysis of FXIII. Variations within the mass spectra of FXIII(a) provide insight into subtle alterations in conformational dynamics that affect chymotrypsin's ability to hydrolyze backbone amide bonds of the TGase. For example, during IIa activation of FXIII, the amide bond between R^{36} and G^{37} is cleaved, and a chymotryptic digest of $FXIIIa^{IIa}$ does not produce the fragment $Q^{32}-F^{44}$. Proteolysis of $FXIIIa^{IIa}$ by chymotrypsin produces a significant amount of the activation peptide residues $G^{9}-L^{31}$. By contrast, the digests of zymogen and $FXIIIa^{Ca}$ displayed the peptide $Q^{32}-F^{44}$ and less $G^{9}-L^{31}$. In our studies with FXIII(a), significant variation within 30 min of trypsin proteolysis were not observed (data not shown); thus, the focus was centered on chymotryptic digests of FXIII(a). Selected data for chymotrypsin proteolysis is summarized in Figure 7. Within the β sandwich, two peptides were cleaved more effectively with $FXIIIa^{Ca}$: 75−83 and 104−125. $FXIIIa^{IIa}$ displayed a large abundance of the catalytic core fragment 207−214. Finally, two fragments in β barrel 2, 681−691 and 692−698, were more susceptible to chymotrypsin in $FXIIIa^{Ca}$. The inhibitor K9 DON did not significantly affect the chymotryptic digests profiles.

Table 2: Cysteine Alkylation Results at pH 8.3

cysteine residues	152[a]	188	238	314[c]	327	374	409	423	695
zymogen		X[b]							
$FXIIIa^{Ca}$		X		X					X
IAA $FXIIIa^{Ca}$		X		IAA			X		X
K9 DON $FXIIIa^{Ca}$		X	weak	K9 DON					X
$FXIIIa^{IIa}$			X	X	X		X		
IAA $FXIIIa^{IIa}$			X	IAA	X		X		
K9 DON $FXIIIa^{IIa}$		X	X	K9 DON	X		weak		X

[a] A blank space indicates that the modified peaks were *not* observed in the mass spectra. [b] NEM modification of cysteine was identified. [c] Cysteine 314 in the activated state reacted with NEM in the uninhibited forms. The presence of the inhibitor covalently linked to cysteine 314 prevented NEM from modifying the active site, and the NEM peak was unobserved in the mass spectra.

Table 3: Lysine Acetylation Results for FXIIIa^{Ca}

	β sandwich								catalytic core						
residues	54[a]	68	73	113	129	133	151	156	199	221	257	482	503	504	513
zymogen	X[b]			?[c]	X	X								?	?
FXIIIa^{Ca}	X		X	X		X	?	X	X	X	X	X	?	?	?
IAA FXIIIa^{Ca}	X		X	X		X	?	X	X	X	X	X	?	?	
K9 DON FXIIIa^{Ca}	X		X	X		X	?	X	X	X	X			?	?

	β barrel 1								β barrel 2				
residues	531	534	565	569	570	583	584	621	623	635	677	678	704
zymogen	?	X				X	X	X	X	X	?	?	X
FXIIIa^{Ca}	X	X	X		X	X	X	X	X	X	?	?	X
IAA FXIIIa^{Ca}	X	X	?	?	X	X	X	X	X	X	?	?	X
K9 DON FXIIIa^{Ca}	X	X	X	?	?	X	X	X	X	X	?	?	X

[a] Residues displaying modification regardless of FXIII activation or inhibition are referred to as always solvent exposed. [b] The letter X represents lysine modification of the indicated residue. [c] A question mark denotes ambiguous data and that the possibility exists for modification of the lysine residue. The first possibility is when two peptides have similar masses and both possess lysine residues. Alternatively, a peptide with two or three lysine residues may be observed as acetylated once, thus presenting ambiguity in assigning the modified lysine.

Table 4: Lysine Acetylation Results for FXIIIa^{IIa}

	β sandwich								catalytic core						
residues	54[a]	68	73	113	129	133	151	156	199	221	257	482	503	504	513
zymogen	X[b]			?[c]	X	X								?	?
FXIIIa^{IIa}	X	X	X	X	X	X	?	X	X	X	X	X	X	X	X
IAA FXIIIa^{IIa}	X	X	X	X	X	X	?	X	X	X	X	X	X	X	X
K9 DON FXIIIa^{IIa}	X	X	X	X	X	X	?	X	X	X	X	X	X	X	X

	β barrel 1								β barrel 2				
residues	531	534	565	569	570	583	584	621	623	635	677	678	704
zymogen	?	X				X	X	X	X	X	?	?	X
FXIIIa^{IIa}	X	X	X	?	?			X	X	X	?	?	X
IAA FXIIIa^{IIa}	X	X	X						X	X	?	?	X
K9 DON FXIIIa^{IIa}	X	X	?	?	?				X	X	?	?	X

[a] Residues displaying modification regardless of FXIII activation or inhibition are referred to as always solvent exposed. [b] The letter X represents lysine modification of the indicated residue. [c] A question mark denotes ambiguous data and that the possibility exists for modification of the lysine residue. The first possibility is when two peptides have similar masses and both possess lysine residues. Alternatively, a peptide with two or three lysine residues may be observed as acetylated once, thus presenting ambiguity in assigning the modified lysine.

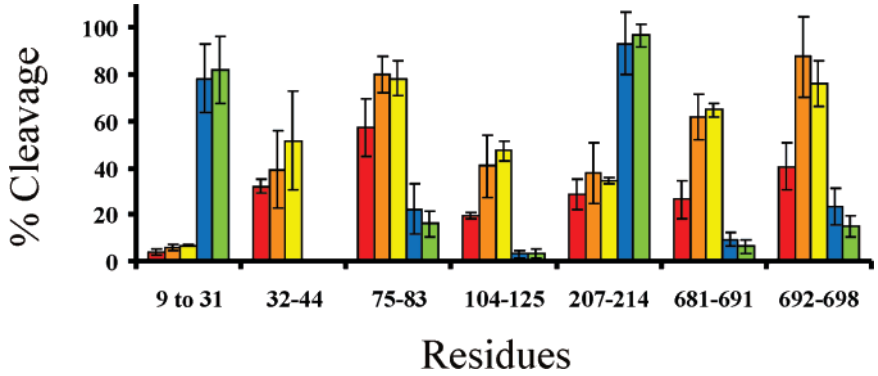

FIGURE 7: Graph of limited chymotryptic proteolysis of FXIII. Only differences in proteolysis larger than ±20% were considered significant. The colored bars refer to the zymogen (red), FXIIIa^{Ca} (orange), K9 DON FXIIIa^{Ca} (yellow), FXIIIa^{IIa} (blue), and K9 DON FXIIIa^{IIa} (green). Errors correspond to the standard deviation of the mean for three independent trials.

DISCUSSION

At the present time, an X-ray structure of FXIIIa interacting with a substrate or inhibitor has not been solved. Furthermore, limited evidence exists on how Q containing substrates access the active site, interact with the catalytic core, and alter the dynamics of FXIIIa in preparation for the K containing substrate (Figure 1). An effective peptide inhibitor for FXIIIa has now been developed that incorporates the glutamine isostere 6-diazo-5-oxo-norleucine into the FXIIIa substrate peptide K9. The focus of the work has proceeded to observe *in solution* the conformational changes associated with inhibition by K9 DON compared to that by IAA. In addition to probing FXIIIa inhibition, new insight has also been obtained regarding the conformational features associated with the activation of FXIIIa by Ca^{2+} and by IIa, thus augmenting our previous investigations (*22*, *23*). The current studies thus provide valuable information about events occurring in the β sandwich, the activation peptide, the dimer interface, the catalytic core, and β barrels 1 and 2.

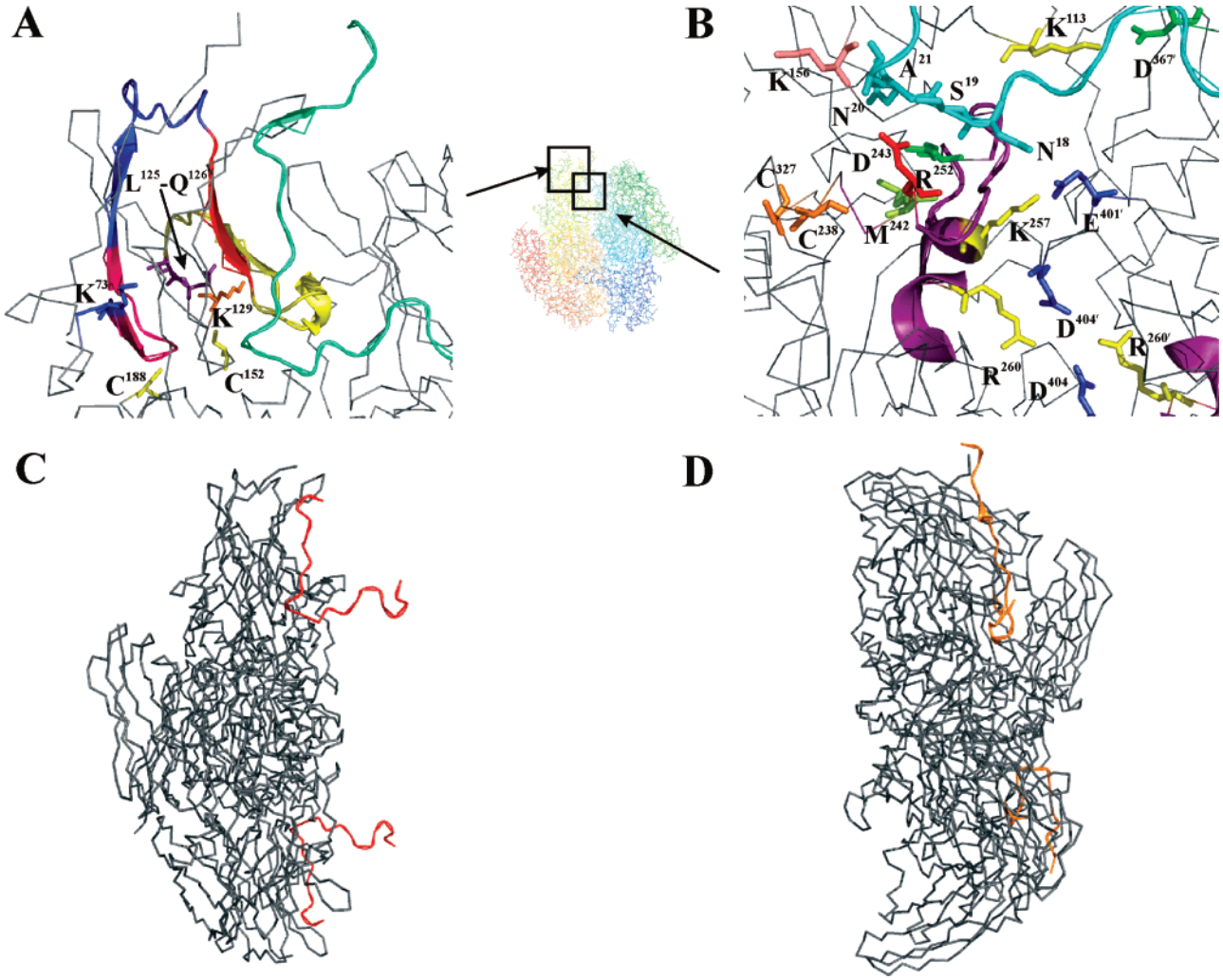

FIGURE 8: Illustration of FXIII (1FIE) regions where activation or inhibitor binding resulted in the described conformational changes. (A) β sandwich region: depicted are the activation peptide (cyan), peptide 4 fragments 72−74/84−97 and K^{73} (blue), limited proteolysis fragments 75−83 (pink) and 104−125 (yellow), L^{125}−Q^{126} (purple), K^{129} (orange), the HDX fragment 98−104 (red), and C^{152}/C^{188} (yellow). (B) Activation peptide/dimer interface: residues N^{18}/S^{19}/N^{20}/A^{21} (cyan), K^{156} (pink), D^{243} (red), R^{252} (dark green), M^{242} (green), C^{238}/C^{327} (orange), the HDX fragments 240−247 and 248−264 (purple), K^{113}/K^{257}/R^{260} (yellow), $D^{367'}$ (green), and $E^{401'}$/$D^{404'}$ (blue). (C) Zymogen crystal structure 1GGT (*5*) displaying the activation peptide (red) extending away from the dimer. (D) $FXIIIa^{IIa}$ crystal structure 1FIE (*10*) (orange) displaying the activation peptide resting across the surface of the dimer. These figures were made using PyMol (*6*).

DON Inhibition of $FXIIIa^{IIa}$. A modified version of the Dade−Behring Berichrom assay (*19*) was used to determine that K9 DON is a slightly less potent inhibitor of $FXIIIa^{IIa}$ as compared to IAA. A longer peptide derived from the natural substrate α_2 antiplasmin has been reported to be an even better FXIIIa substrate model. α_2AP (1−15) shows improved kinetic parameters, maintains a preference for Q^2 over Q^4, and suggests the existence of additional substrate specificity determinants within the active site (*41*). Incorporation of DON into such a longer peptide sequence could later offer more potent inhibition of FXIIIa as well as contribute to further understanding FXIIIa−ligand interactions. The research with K9 DON provides our first successful application of such a peptide inhibitor to probe changes occurring in the FXIIIa conformation in solution.

β Sandwich and Proteolytic Versus Non-Proteolytic Activation. The β sandwich residues 72−97, also known as peptide 4, are hypothesized to be involved in Q substrate recognition (Figures 1A and 8A) since synthetic peptides derived from this sequence compete for Q substrate binding to FXIIIa (*20*). An earlier report demonstrated that K^{73} was acetylated in only $FXIIIa^{Ca}$ (*23*). The present results confirm this finding as well as showing that $FXIIIa^{IIa}$ is also modified at this position. The current research further indicates that $FXIIIa^{Ca}$ exhibits increased chymotryptic proteolysis of residues 75−83 within this peptide 4 region. Together, these results suggest increased exposure of the 73−83 region upon activation, especially for $FXIIIa^{Ca}$. These events could signal FXIIIa preparation for Q substrate interaction with the β sandwich (*20*).

Other unique properties related to $FXIIIa^{Ca}$ include an increase in the proteolysis of the 104−125 segment, a loss of the ability to acetylate K^{129}, and a protection from solvent for residues 98−104. As the L^{125}−Q^{126} peptide bond becomes more accessible to chymotrypsin, it may be at the expense of K^{129} solvent exposure. Between peptide 4 (72−97) and the chymotryptic cleavage region (104−125) is the segment 98−104. Previous HDX studies have demonstrated that residues 98−104 of $FXIIIa^{Ca}$ exhibited a significant decrease in deuteration that may be localized to L^{98} and F^{99} (Figure 8A) (*22*). IAA inhibition of $FXIIIa^{Ca}$ further stabilizes this short segment from deuteration. K9 DON $FXIIIa^{Ca}$

requires more time to achieve significant stabilization of this fragment conceivably due to allostery related to peptide binding within the catalytic core. Interestingly, the 98−104 fragment is not observed in the peptic digest of FXIIIa^{IIa} used for the HDX studies.

The differences in proteolysis observed for FXIIIa^{Ca} versus FXIIIa^{IIa} are important to consider. With both chymotrypsin and pepsin, fewer cleavages are detected within the β sandwich region of FXIIIa^{IIa}. Cleavage of the activation peptide by IIa may thus protect certain regions within the β sandwich. Alternatively, the potential presence of low affinity Ca^{2+} binding site(s) within this domain could aid in creating a more accessible environment for the proteases to cleave FXIIIa^{Ca}. An earlier study ascertained that IAA FXIIIa^{IIa} possessed a higher affinity for fibrin II than for IAA FXIIIa^{Ca} (*42*). Another investigation found that FXIIIa^{Ca} was unable to cross-link fibrin α chains, while retaining the ability to cross-link fibrin γ chains (*43*). Perhaps several fibrin binding sites are located in or influenced by the β sandwich, and only cleavage of the activation peptide is able to properly orient or expose residues related to fibrin α chain binding.

FXIII Activation Peptide and the Dimer Interface. Located in close proximity to the activation peptide and the dimer interface, FXIIIa fragments 240−247 and 248−264 became more exposed to deuterium when compared to zymogen (Figure 8B). In addition, acetylation of K^{113}, K^{156}, and K^{257} only occurred when FXIII was activated. Several electrostatic and water mediated interactions are apparent between the activation peptide residues N^{18}−A^{21} and main chain residues K^{156}, D^{243}, and R^{252}. The crystal structures of zymogen (1GGT) (*5*) and FXIIIa^{IIa} (1FIE) (*10*) display the activation peptide in similar conformations except for one key stretch. The N-terminus of zymogen (F^{8}−P^{16}) is extended away from the dimer, while in FXIIIa^{IIa}, these same residues are depicted as resting on the dimer's surface (Figure 8C and D). Perhaps this emphasizes the importance of N^{18}−A^{21} in anchoring the activation peptide to FXIII through interactions with K^{156}, D^{243}, and R^{252}.

Alkylation of the adjacent residues C^{238} and C^{327} occurred only with FXIIIa^{IIa} (Figure 8B). C^{238} is involved in main chain H bonding with M^{242}, adjacent to D^{243}. Cleavage of the activation peptide could conceivably weaken the aforementioned electrostatic interactions involving residues within 240−264 and the activation peptide, essentially perturbing the dynamics of this region. In fact, limited proteolysis of FXIIIa^{IIa} shows a large abundance of the fragment 9−31. As stated in the previous section, these observations could signal FXIIIa^{IIa} preparation for efficient interaction with the α chains of fibrin. The FXIII mutations M^{242}T, R^{252}I, and G^{262}E further highlight the structural and functional importance for this stretch of catalytic core residues (*44*−*46*).

Intersubunit H bonding among K^{113}−D$^{367'}$, K^{257}−E$^{401'}$, and R^{260}−D$^{404'}$ emphasize the role these residues play in maintaining dimer integrity (Figures 1B and 8B). Acetylation of K^{113} and K^{257} and the increased exposure of 248−264 insinuate an opening of the dimer space. Yee et al. predict a possible mode of the K substrate accessing the active site through the opening of the dimer interface (*5*). Our results suggest that activation of FXIII weakens the interactions between residues at the dimer interface. These observations are consistent with K-containing substrates accessing the active site from the dimer interface, where, as previously suggested, the acyl acceptor is directed to the active site by residue D^{343} and the H^{342}/E^{434} diad (*5*). Three reported mutations resulting in congenital FXIII deficiency, R^{260}L, R^{260}C, and R^{260}H, signify the essential nature of the R^{260}−D$^{404'}$ interaction for proper FXIII functioning (*47*−*50*).

cis−*trans Isomerization Within the Catalytic Core and the Secondary IIa Cleavage Site*. NEM modification of C^{409} was severely impaired by the covalent linkage of K9 DON to C^{314} in both FXIIIa^{Ca} and FXIIIa^{IIa} (Figure 9B). Two nonprolyl *cis* bonds, Q^{425}−F^{426} and R^{310}−Y^{311}, reside near C^{314} and C^{409}. These unusual *cis* peptide bonds may possess ample potential energy that an enzyme such as FXIII could use to fuel the TGase reaction and/or open access for substrates within the active site (*51*). The Ahvazi group, through molecular modeling studies on the related species tissue TGase 1 and 3, suggest that Ca^{2+} binding stabilizes the non prolyl *cis* bonds in preparation for catalysis and that Q substrate binding results in the *cis*−*trans* isomerization (*52*, *53*). C^{409} may no longer be available for alkylation by NEM as a result of Q^{425}−F^{426} isomerization, which resides about 6.5 Å from C^{409}. An alternative explanation could be that K9 DON interacts near or with C^{409}. The distance between C^{314} and C^{409} is about 13 Å, indicating that the five C-terminal residues (−SLVIG) of the inhibitor would have to exist in an extended conformation (approximately 20 Å in length) toward the dimer interface. This hypothesis is supported by recent transferred NOESY data that suggest that the β casein derived FXIIIa substrate K9 and an α_2 antiplasmin peptide adopted extended conformations within the active site of FXIIIa^{IIa} (*41*).

Another interesting observation was that K^{482} and K^{503} were not modified in K9 DON FXIIIa^{Ca}. K^{482} is located near the Ca^{2+} binding site, and K^{503} resides on a fragment leading to β barrel 1 near the FXIII secondary cleavage site (K^{513}−S^{514}). Unfortunately, fragments resulting from tryptic proteolysis of K^{513}−S^{514} rarely appeared in the mass spectra after a 30 min digest. Nevertheless, the acetylation results suggest that K9 DON inhibition may act in concert with Ca^{2+} binding to protect against further proteolysis at the secondary cleavage site by IIa.

FXIIIa^{IIa}: The Peptide 7 Region and Catalytic Core. The fragment 220−230 within the potential Q substrate recognition site known as peptide 7 (190−230) (*20*) experienced similar levels of deuterium incorporation upon inhibition, as also seen with activation. Furthermore, acetylation of both K^{221} and K^{199} only occurs in FXIIIa. Inhibition of FXIIIa did not result in hindering the modification of these residues. These findings are consistent with any of the following conclusions: residues 220−230, K^{199}, and K^{221} are not involved in direct substrate recognition, a 10-residue peptide is not of sufficient length to reach peptide 7, and/or Q-containing substrates do not lead to allosteric effects within these regions.

Unique to FXIIIa^{IIa} was the increased proteolysis of the peptide 7 residues 207−214 by chymotrypsin and acetylation of K^{68} (Figure 9D). The distance from the side chain of K^{68} to the backbone carbonyl of L^{206} is 3.8 Å, suggesting H bond disruption concurrent with IIa activation. A highly conserved loop among all TGases exists between residues 467−472, which appear to shield a portion of peptide 7. Our lab's previous observation that K^{467} was acetylated upon activation (*23*) indicates a possible rearrangement of this K^{467} loop.

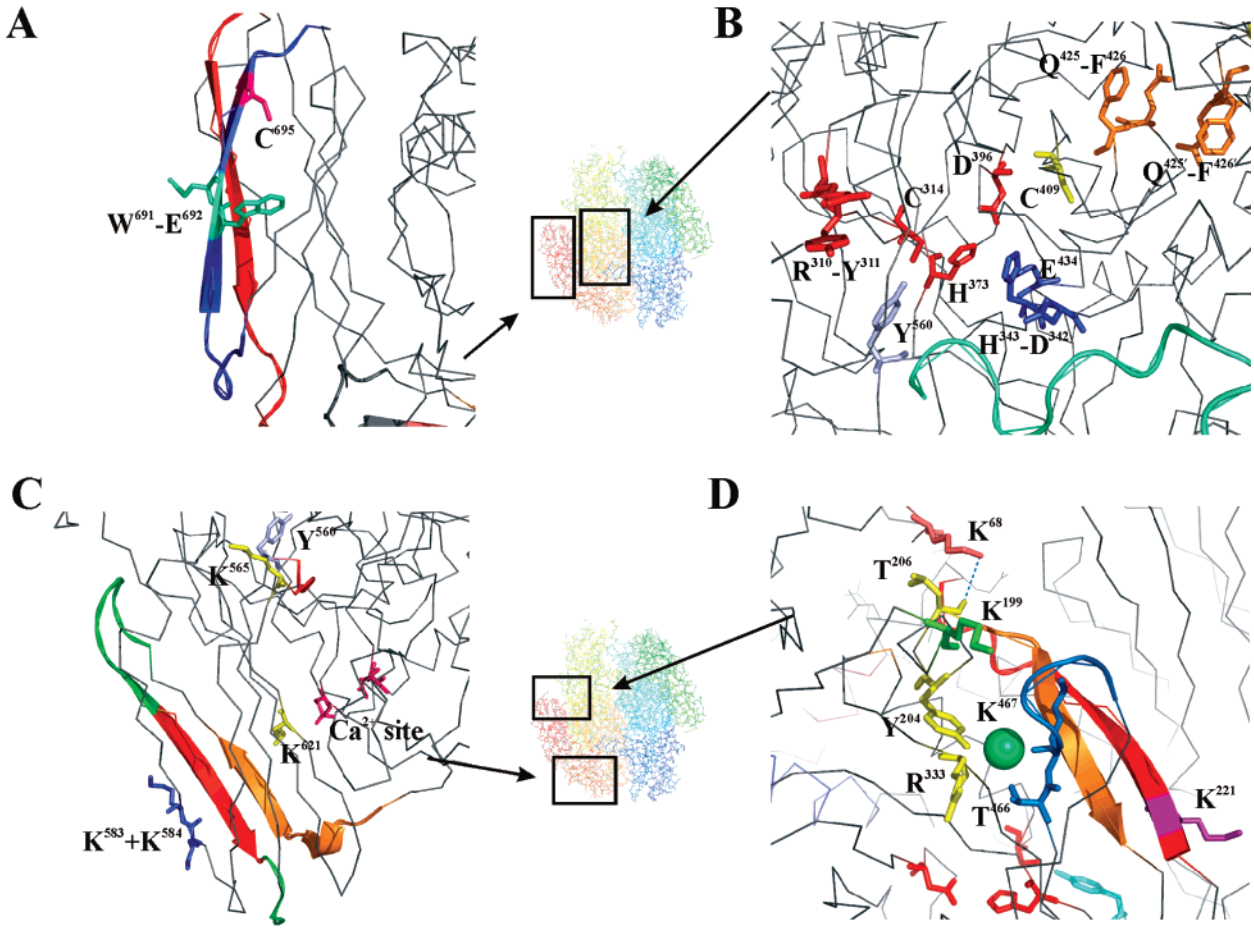

FIGURE 9: Illustration of FXIII (1FIE) regions, where activation or inhibitor binding resulted in the described conformational changes. (A) β barrel 2: the 5A2 binding epitope (red), the limited proteolysis fragment 681−698 (blue), W^{691}−E^{692} (cyan), and C^{695} (red). (B) Catalytic Core I: the activation peptide (cyan), $D^{342}/H^{343}/E^{434}$ (blue), Y^{560} (light blue), $C^{314}/H^{373}/D^{396}$ (red), C^{409} (yellow), and the non-prolyl *cis* bonds R^{310}−Y^{311} (red) and Q^{425}−F^{426} (orange). (C) β barrel 1: the HDX fragments 526−534/542−546 (green), 535−541 (red), and 513−522 (orange), K^{565}/K^{621} (yellow), Y^{560} (light blue), 561−564 (red), K^{583}/K^{584} (blue), and the Ca^{2+} binding site (pink). (D) Catalytic Core II: HDX fragment 220−230 (red), limited proteolysis fragment 207−214 (orange), and residues K^{199} (green), K^{221} (purple), K^{68} (red), T^{206} (yellow), Y^{204}/R^{333} (yellow), and 466−472 (blue). These figures were made using PyMol (*6*).

Curiously, Fox et al. noticed a highly conserved water at a fork between two β strands (*13*), which is situated within a pocket formed by the conserved residues Y^{204}, R^{333}, T^{466}, and K^{467}. Fox et al. also observed that the strand containing R^{333} runs antiparallel to the strand with H^{373} and that T^{466}/K^{467} are downstream of A^{457}, a Ca^{2+} binding site residue (*13*). This potential K^{467} loop repositioning could be associated with the increased exposure of peptide 7 and proper orientation of residues involved in catalysis. A study examining the consequences of TGase 1 mutations resulting in rare skin disorders commented on the significance of an R^{395}L (R^{333} in FXIII) mutant on impairing TGase 1 activity (*54*). Also, the FXIII polymorphism Y^{204}F leads to higher occurrences of recurrent miscarriage, probably because of conformational changes resulting from the disruption of Y^{204}−R^{333} H bonding (*55*).

Ca^{2+} Concentration and FXIIIa Inhibition Affect Dynamics of β Barrel 1. The current HDX results confirm an earlier report of Ca^{2+} protecting the fragments 513−522 and 526−546 from deuterium exchange (*22*); however, $FXIIIa^{Ca}$ displayed significantly more protection from solvent within this region than $FXIIIa^{IIa}$ (Table 1). Fragment 535−541 remained at similar deuterium levels compared to those of zymogen, which enabled the observed changes in dynamics to be localized to the two flanking loops, 526−534 and 542−546 (Figure 9C). The isotopic cluster for FXIII residues 526−546 exposed to 1 mM Ca^{2+} appears to be an amalgam of zymogen and $FXIIIa^{Ca}$ (Figure 6). This isotopic cluster possibly illustrates a concentration of Ca^{2+}, where the cation binding site is not fully occupied. Analysis of these results could be interpreted to signify allostery within TGase. Ca^{2+} binding could potentially direct β barrel 1 to roll away from the catalytic core to allow Q substrate access, as previously hypothesized (*10*).

Interestingly, the presence of K9 DON results in increased protection for 526−546 from solvent after 10 min in both $FXIIIa^{Ca}$ and $FXIIIa^{IIa}$. Even residues 513−522, though only in $FXIIIa^{IIa}$, were slightly more protected in the presence of either K9 DON or IAA (Table 1). Both of these inhibitors also blocked lysine acetylation of K^{621} in $FXIIIa^{IIa}$. These results suggest that Q substrate binding further stabilizes β barrel 1, perhaps restricting access to additional Q substrates in preparation for covalent cross-linking to the acyl acceptor.

Is β Barrel 2 the Location of a Lysine-Containing Substrate Recognition Site? Within β barrel 2, chemical modification studies have provided evidence for C^{695} exposure concurrent with activation (*23*). In the current work, only $FXIIIa^{Ca}$ was always alkylated at C^{695} regardless of inhibition, while $FXIIIa^{IIa}$ alkylation occurred when K9 DON was present at the active site. The discrepancy in our results

is likely due to the amount of NEM used in our earlier report (200 mM vs 50 mM) (*23*). Further supporting this finding was the limited proteolysis studies demonstrating that $FXIIIa^{Ca}$ resulted in increased chymotryptic proteolysis of $W^{691}-E^{692}$, which may be related to C^{695} exposure (Figure 9A).

As illustrated in Mitkevich et al., the antibody 5A2 that targets the FXIIIa epitope 646−658 displays uncompetitive inhibition toward the Q substrate and competitive inhibition against the K substrate (*21*). In fact, 5A2 binding is enhanced when the acyl donor binds to the active site (*21*). The K9 DON $FXIIIa^{IIa}$ results suggest that the Q substrate creates a more solvent accessible region within β barrel 2, potentially involved in K substrate recognition. This hypothesis is in line with competitive inhibition of the acyl acceptor reaction when 5A2 binds to the FXIIIa epitope 646−658 (*21*).

CONCLUSIONS

The main objectives of this project were to demonstrate the applicability of DON based peptides in FXIIIa inhibition and to explore perturbations associated with activation and inhibition on FXIIIa dynamics. For the first time, our chemical modification and newly implemented limited proteolysis studies utilized the protease chymotrypsin in addition to trypsin. These results corroborate and further augment previous FXIII studies from our lab (*22*, *23*).

New insight was obtained into the conformational variance among $FXIIIa^{Ca}$ and $FXIIIa^{IIa}$. Chymotrypsin proteolysis supplied evidence of additional peptide 7 exposure resulting from IIa activation: the fragment 207−214 is cleaved more efficiently, and K^{68} is acetylated in $FXIIIa^{IIa}$. Also with $FXIIIa^{IIa}$, increased proteolysis of 9−31 and alkylation of the nearby residues C^{238}/C^{327} suggest unique events associated with activation of peptide cleavage. $FXIIIa^{Ca}$ revealed amplification in proteolysis of the peptide bond $L^{125}-Q^{126}$ and suppression of nearby K^{129} acetylation. The β barrel 2 peptide bond $W^{691}-E^{692}$ and C^{695} in $FXIIIa^{Ca}$ were more solvent accessible than with $FXIIIa^{IIa}$. These results perhaps indicate allostery associated with Ca^{2+} binding or the presence of additional Ca^{2+} binding sites within these domains. Regardless of the activation method, FXIIIa experienced an increase in deuteration for 240−268 and was modified at K^{113}, K^{156}, and K^{257}. These events could indicate opening of the dimer interface for K substrate access to the active site.

With regard to FXIIIa inhibition, our results demonstrate that K9 DON is an effective inhibitor of $FXIIIa^{IIa}$. Furthermore, the solution studies reveal potential conformational features of FXIIIa trapped in the active state by K9 DON and IAA. Specific to K9 DON inhibition was the cessation of C^{409} alkylation within the active site, unique perturbations of deuterium incorporation for the β sandwich fragment 98−104 from $FXIIIa^{Ca}$, increased accessibility of C^{695} with $FXIIIa^{IIa}$, and blocked K^{482}/K^{503} acetylation in $FXIIIa^{Ca}$. General inhibition resulted in the $FXIIIa^{IIa}$ residue K^{621} no longer being available for acetylation and the β barrel 1 fragments 513−522 and 526−546 becoming more protected from deuteration. These observations provide subtle glimpses into how substrate bound FXIIIa prepares for the incoming lysine-containing substrate. The current work focuses on the consequences of interactions at the active site of FXIIIa. Future endeavors into FXIII dynamics will examine larger more physiologically based substrates potentially evoking greater conformational changes and further targeting of putative binding exosites.

ACKNOWLEDGMENT

We are grateful for the gift of recombinant FXIII A_2 from Paul Bishop of Zymogenetics, Inc, Seattle, WA. G. Isetti began the initial explorations into the K9 DON project, and for this, we are deeply indebted. We are appreciative of valuable contributions to the HDX procedure and to prior investigations of FXIII dynamics by B. T. Turner, Jr. Also, we acknowledge the improvements in the NEM protocol made by E. Saunders. Finally, we thank D. B. Cleary for the critical evaluation of the current project.

SUPPORTING INFORMATION AVAILABLE

Tables S1 and S2 present the amount of total deuterium incorporation for FXIII at 1 and 10 min, respectively. Figure S1 illustrates the FXIII sequence coverage obtained with pepsin, trypsin, and chymotrypsin. This material is available free of charge via the Internet at http://pubs.acs.org.

REFERENCES

1. Weisel, J. W. (2005) Fibrinogen and fibrin, *Adv. Protein Chem. 70*, 247−299.
2. Lane, D. A., Philippou, H., and Huntington, J. A. (2005) Directing thrombin, *Blood 106*, 2605−2612.
3. Lorand, L., and Graham, R. M. (2003) Transglutaminases: crosslinking enzymes with pleiotropic functions, *Nat. Rev. Mol. Cell Biol. 4*, 140−156.
4. Ritchie, H., Lawrie, L. C., Crombie, P. W., Mosesson, M. W., and Booth, N. A. (2000) Cross-linking of plasminogen activator inhibitor 2 and alpha 2-antiplasmin to fibrin(ogen), *J. Biol. Chem. 275*, 24915−24920.
5. Yee, V. C., Pedersen, L. C., Le Trong, I., Bishop, P. D., Stenkamp, R. E., and Teller, D. C. (1994) Three-dimensional structure of a transglutaminase: human blood coagulation factor XIII, *Proc. Natl. Acad. Sci. U.S.A. 91*, 7296−7300.
6. DeLano, W. L. (2002) *The PyMOL Molecular Graphics System*, DeLano Scientific, San Carlos, CA.
7. Pedersen, L. C., Yee, V. C., Bishop, P. D., Le, Trong, I., Teller, D. C., and Stenkamp, R. E. (1994) Transglutaminase factor XIII uses proteinase-like catalytic triad to crosslink macromolecules, *Protein Sci. 3*, 1131−1135.
8. Lorand, L., and Konishi, K. (1964) Activation of the fibrin stabilizing factor of plasma by thrombin, *Arch. Biochem. Biophys. 105*, 58−67.
9. Hornyak, T. J., and Shafer, J. A. (1991) Role of calcium ion in the generation of factor XIII activity, *Biochemistry 30*, 6175−6182.
10. Yee, V. C., Pedersen, L. C., Bishop, P. D., Stenkamp, R. E., and Teller, D. C. (1995) Structural evidence that the activation peptide is not released upon thrombin cleavage of factor XIII, *Thromb. Res. 78*, 389−397.
11. Polgar, J., Hidasi, V., and Muszbek, L. (1990) Non-proteolytic activation of cellular protransglutaminase (placenta macrophage factor XIII), *Biochem. J. 267*, 557−560.
12. Curtis, C. G., Brown, K. L., Credo, R. B., Domanik, R. A., Gray, A., Stenberg, P., and Lorand, L. (1974) Calcium-dependent unmasking of active center cysteine during activation of fibrin stabilizing factor, *Biochemistry 13*, 3774−3780.
13. Fox, B. A., Yee, V. C., Pedersen, L. C., Le Trong, I., Bishop, P. D., Stenkamp, R. E., and Teller, D. C. (1999) Identification of the calcium binding site and a novel ytterbium site in blood coagulation factor XIII by X-ray crystallography, *J. Biol. Chem. 274*, 4917−4923.
14. Lewis, B. A., Freyssinet, J. M., and Holbrook, J. J. (1978) An equilibrium study of metal ion binding to human plasma coagulation factor XIII, *Biochem. J. 169*, 397−402.
15. Ambrus, A., Banyai, I., Weiss, M. S., Hilgenfeld, R., Keresztessy, Z., Muszbek, L., and Fesus, L. (2001) Calcium binding of

transglutaminases: a 43Ca NMR study combined with surface polarity analysis, *J. Biomol. Struct. Dyn. 19*, 59−74.
16. Hornyak, T. J., Bishop, P. D., and Shafer, J. A. (1989) Alpha-thrombin-catalyzed activation of human platelet factor XIII: relationship between proteolysis and factor XIIIa activity, *Biochemistry 28*, 7326−7332.
17. Curtis, C. G., Stenberg, P., Chou, C. H., Gray, A., Brown, K. L., and Lorand, L. (1973) Titration and subunit localization of active center cysteine in fibrinoligase (thrombin-activated fibrin stabilizing fector), *Biochem. Biophys. Res. Commun. 52*, 51−56.
18. Hausch, F., Halttunen, T., Maki, M., and Khosla, C. (2003) Design, synthesis, and evaluation of gluten peptide analogs as selective inhibitors of human tissue transglutaminase, *Chem. Biol. 10*, 225−231.
19. Fickenscher, K., Aab, A., and Stuber, W. (1991) A photometric assay for blood coagulation factor XIII, *Thromb. Haemostasis 65*, 535−540.
20. Achyuthan, K. E., Slaughter, T. F., Santiago, M. A., Enghild, J. J., and Greenberg, C. S. (1993) Factor XIIIa-derived peptides inhibit transglutaminase activity. Localization of substrate recognition sites, *J. Biol. Chem. 268*, 21284−21292.
21. Mitkevich, O. V., Shainoff, J. R., DiBello, P. M., Yee, V. C., Teller, D. C., Smejkal, G. B., Bishop, P. D., Kolotushkina, I. S., Fickenscher, K., and Samokhin, G. P. (1998) Coagulation factor XIIIa undergoes a conformational change evoked by glutamine substrate. Studies on kinetics of inhibition and binding of XIIIA by a cross-reacting antifibrinogen antibody, *J. Biol. Chem. 273*, 14387−14391.
22. Turner, B. T. Jr., and Maurer, M. C. (2002) Evaluating the roles of thrombin and calcium in the activation of coagulation factor XIII using H/D exchange and MALDI-TOF MS, *Biochemistry 41*, 7947−7954.
23. Turner, B. T. Jr., Sabo, T. M., Wilding, D., and Maurer, M. C. (2004) Mapping of factor XIII solvent accessibility as a function of activation state using chemical modification methods, *Biochemistry 43*, 9755−9765.
24. Bishop, P. D., Teller, D. C., Smith, R. A., Lasser, G. W., Gilbert, T., and Seale, R. L. (1990) Expression, purification, and characterization of human factor XIII in *Saccharomyces cerevisiae*, *Biochemistry 29*, 1861−1869.
25. Trumbo, T. A., and Maurer, M. C. (2000) Examining thrombin hydrolysis of the factor XIII activation peptide segment leads to a proposal for explaining the cardioprotective effects observed with the factor XIII V34L mutation, *J. Biol. Chem. 275*, 20627−20631.
26. Marinescu, A., Cleary, D. B., Littlefield, T. R., and Maurer, M. C. (2002) Structural features associated with the binding of glutamine-containing peptides to Factor XIII, *Arch. Biochem. Biophys. 406*, 9−20.
27. Brocklehurst, K., and Malthouse, J. P. (1978) Mechanism of the reaction of papain with substrate-derived diazomethyl ketones. Implications for the difference in site specificity of halomethyl ketones for serine proteinases and cysteine proteinases and for stereoelectronic requirements in the papain catalytic mechanism, *Biochem. J. 175*, 761−764.
28. Rajagopal, S., Meyer, S. C., Goldman, A., Zhou, M., and Ghosh, I. (2006) A minimalist approach toward protein recognition by epitope transfer from functionally evolved beta-sheet surfaces, *J. Am. Chem. Soc. 128*, 14356−14363.
29. Seelig, G. F., and Folk, J. E. (1980) Half-of-the-sites and all-of-the-sites reactivity in human plasma blood coagulation factor XIIIa, *J. Biol. Chem. 255*, 9589−9593.
30. Mandell, J. G., Falick, A. M., and Komives, E. A. (1998) Measurement of amide hydrogen exchange by MALDI-TOF mass spectrometry, *Anal. Chem. 70*, 3987−3995.
31. Mandell, J. G., Falick, A. M., and Komives, E. A. (1998) Identification of protein-protein interfaces by decreased amide proton solvent accessibility, *Proc. Natl. Acad. Sci. U.S.A. 95*, 14705−14710.
32. Mandell, J. G., Baerga-Ortiz, A., Akashi, S., Takio, K., and Komives, E. A. (2001) Solvent accessibility of the thrombin-thrombomodulin interface, *J. Mol. Biol. 306*, 575−589.
33. Croy, C. H., Koeppe, J. R., Bergqvist, S., and Komives, E. A. (2004) Allosteric changes in solvent accessibility observed in thrombin upon active site occupation, *Biochemistry 43*, 5246−5255.
34. Mandell, J. G., Baerga-Ortiz, A., Falick, A. M., and Komives, E. A. (2005) Measurement of solvent accessibility at protein-protein interfaces, *Methods Mol. Biol. 305*, 65−80.
35. Koeppe, J. R., Seitova, A., Mather, T., and Komives, E. A. (2005) Thrombomodulin tightens the thrombin active site loops to promote protein C activation, *Biochemistry 44*, 14784−14791.
36. Koeppe, J. R., and Komives, E. A. (2006) Amide H/2H exchange reveals a mechanism of thrombin activation, *Biochemistry 45*, 7724−7732.
37. Sabo, T. M., Farrell, D. H., and Maurer, M. C. (2006) Conformational analysis of gamma′ peptide (410−427) interactions with thrombin anion binding exosite II, *Biochemistry 45*, 7434−7445.
38. Wang, L., Lane, L. C., and Smith, D. L. (2001) Detecting structural changes in viral capsids by hydrogen exchange and mass spectrometry, *Protein Sci. 10*, 1234−1243.
39. Chen, J., and Smith, D. L. (2001) Amide hydrogen exchange shows that malate dehydrogenase is a folded monomer at pH 5, *Protein Sci. 10*, 1079−1083.
40. Ansong, C., Miles, S. M., and Fay, P. J. (2006) Factor VIII A1 domain residues 97−105 represent a light chain-interactive site, *Biochemistry 45*, 13140−13149.
41. Cleary, D. B., and Maurer, M. C. (2006) Characterizing the specificity of activated Factor XIII for glutamine-containing substrate peptides, *Biochim. Biophys. Acta. 1764*, 1207−1217.
42. Hornyak, T. J., and Shafer, J. A. (1992) Interactions of factor XIII with fibrin as substrate and cofactor, *Biochemistry 31*, 423−429.
43. Okada, M., Blomback, B., Chang, M. D., and Horowitz, B. (1985) Fibronectin and fibrin gel structure, *J. Biol. Chem. 260*, 1811−1820.
44. Mikkola, H., Yee, V. C., Syrjala, M., Seitz, R., Egbring, R., Petrini, P., Ljung, R., Ingerslev, J., Teller, D. C., Peltonen, L., and Palotie, A. (1996) Four novel mutations in deficiency of coagulation factor XIII: consequences to expression and structure of the A-subunit, *Blood 87*, 141−151.
45. Onland, W., Boing, A. N., Meijer, A. B., Schaap, M. C., Nieuwland, R., Haasnoot, K., Sturk, A., and Peters, M. (2005) Congenital deficiency of factor XIII caused by two missense mutations in a Dutch family, *Haemophilia 11*, 539−547.
46. Mikkola, H., Syrjala, M., Rasi, V., Vahtera, E., Hamalainen, E., Peltonen, L., and Palotie, A. (1994) Deficiency in the A-subunit of coagulation factor XIII: two novel point mutations demonstrate different effects on transcript levels, *Blood 84*, 517−525.
47. Vysokovsky, A., Saxena, R., Landau, M., Zivelin, A., Eskaraev, R., Rosenberg, N., Seligsohn, U., and Inbal, A. (2004) Seven novel mutations in the factor XIII A-subunit gene causing hereditary factor XIII deficiency in 10 unrelated families, *J. Thromb. Haemostasis 2*, 1790−1797.
48. Peyvandi, F., Tagliabue, L., Menegatti, M., Karimi, M., Komaromi, I., Katona, E., Muszbek, L., and Mannucci, P. M. (2004) Phenotype-genotype characterization of 10 families with severe a subunit factor XIII deficiency, *Hum. Mutat. 23*, 98.
49. Ichinose, A., Tsukamoto, H., Izumi, T., Yamazaki, T., Togashi, M., Takamatsu, J., Saito, H., and Umeyama, H. (1998) Arg260-Cys mutation in severe factor XIII deficiency: conformational change of the A subunit is predicted by molecular modelling and mechanics, *Br. J. Haematol. 101*, 264−272.
50. Kangsadalampai, S., Chelvanayagam, G., Baker, R., Tiedemann, K., Kuperan, P., and Board, P. G. (1999) Identification and characterization of two missense mutations causing factor XIIIA deficiency, *Br. J. Haematol. 104*, 37−43.
51. Weiss, M. S., Metzner, H. J., and Hilgenfeld, R. (1998) Two non-proline cis peptide bonds may be important for factor XIII function, *FEBS. Lett. 423*, 291−296.
52. Boeshans, K. M., Mueser, T. C., and Ahvazi, B. (2007) A three-dimensional model of the human transglutaminase 1: insights into the understanding of lamellar ichthyosis, *J. Mol. Model. (Online) 13*, 233−246.
53. Ahvazi, B., and Steinert, P. M. (2003) A model for the reaction mechanism of the transglutaminase 3 enzyme, *Exp. Mol. Med. 35*, 228−242.
54. Laiho, E., Ignatius, J., Mikkola, H., Yee, V. C., Teller, D. C., Niemi, K. M., Saarialho-Kere, U., Kere, J., and Palotie, A. (1997) Transglutaminase 1 mutations in autosomal recessive congenital ichthyosis: private and recurrent mutations in an isolated population, *Am. J. Hum. Genet. 61*, 529−538.
55. Anwar, R., Gallivan, L., Edmonds, S. D., and Markham, A. F. (1999) Genotype/phenotype correlations for coagulation factor XIII: specific normal polymorphisms are associated with high or low factor XIII specific activity, *Blood 93*, 897−905.

BI700579Z